Research paper

Photosensitizing role of R-phycoerythrin red protein and β-carboline alkaloids in Dye sensitized solar cell. Electrochemical and spectroscopic characterization

Juan G. Yañuk [b], Franco M. Cabrerizo [b,*], Fernando G. Dellatorre [c,d], María F. Cerdá [a,*]

[a] *Laboratorio de Biomateriales, Facultad de Ciencias, UdelaR, Iguá, 4225. 11400 Montevideo, Uruguay*
[b] *Instituto Tecnológico de Chascomús (INTECH), Universidad Nacional de San Martín (UNSAM) – Consejo Nacional de Investigaciones Científicas y Técnicas (CONICET), Av. Intendente Marino, Km 8.2, CC 164 (B7130IWA), Chascomús, Argentina*
[c] *Grupo de Investigación y Desarrollo Tecnológico en Acuicultura y Pesca (GIDTAP), Facultad Regional Chubut, Universidad Tecnológica Nacional, Av. del Trabajo 1536 (9120), Puerto Madryn, Chubut, Argentina*
[d] *Centro de Estudio de Sistemas Marinos (CESIMAR-CONICET), Bvd. Brown 2915 (9120), Puerto Madryn, Chubut, Argentina*

A B S T R A C T

Dye-sensitized solar cell (DSSC) technology represents a valuable source for renewable energy production. Although with a rather low conversion efficiency, the continuous improvement of the price/performance ratio is making this technology more competitive than other sources of electrical power generation. To date, one of the major challenges is the search of novel and low-cost photosensitizers, a key player in the overall photo-conversion process. Natural dyes have shown to be an excellent alternative that still needs to be further explored. In this work, the spectroscopic and electrochemical properties of two different families of naturally occurring pigments (*i.e*, β-carboline alkaloids (βCs) and the red protein R-phycoerythrin (**R-PE**)) as well as their role in DSSCs are addressed. DSSC assemblies show that **R-PE** represents a highly suitable photosensitizer showing quite a high stability with a relative high solar energy to electricity conversion efficiency ($\eta = 0.11$ %) when comparing with other recombinant proteins ($\eta = 0.30$ %). Algae extracts used without further purification showed herein the highest efficiencies. The latter fact has a concomitant positive effect on the overall production cost of these photovoltaic cells. Surprisingly, and despite their positive effect on the coating of the semiconductor surface, the use of βCs as additive decreases the overall conversion efficiency of the **R-PE** based DSSCs evaluated. Data support the hypothesis these alkaloids would be blocking the incident UVB/UVA radiation.

1. Introduction

In most Latin-American countries, the installed capacity for energy production is mainly based on thermal and hydraulic technologies ($\sim$45%–65% and $\sim$35%–45%, respectively).[1,2] The contribution of other sources of energy varies among the countries. In the case of Argentina, nuclear energy represents the 4.2%, whereas wind and solar renewable energies only represent 0.5%.[2] In particular solar power (mainly based on silicon technologies) covers less than $\sim$0.05% of the real energy demand. Instead, Uruguay's energetic matrix is in a frank growth towards renewable energies such as biomass (43%), wind (6%) and solar (1%) power, at expense of the fossil-based technology.[3]

Solar power certainly represents a renewable source with a great potential to drive a change in the global energy matrix towards more sustainable and economically viable technologies. This fact becomes more relevant in developing countries, such as Argentina and Uruguay, where the geographical and climate conditions also provide excellent opportunities for relative short energy payback times. However, the investment on solar technologies in these countries is still very low, mainly due to the fact that production and/or installation costs are still a challenge.

* Corresponding authors.
  E-mail addresses: fcabrerizo@intech.gov.ar (F.M. Cabrerizo), fcerda@fcien.edu.uy (M.F. Cerdá).

[1] In the particular case of Argentina thermal and hydraulic energy production represent the 651% and 302%, respectively; whereas in Uruguay data reported are 36% and 45%, respectively.

[2] Data obtained from the 2017 annual report published by CAMMESA (Compañía Administradora del Mercado Mayorista Eléctrico S. A.).

[3] Data obtained from the 2017 annual report (Balance Energetico Nacional 2017) published by the Uruguay Ministry of Industry, Energy and Mining.

Dye sensitized solar cells (DSSCs) has a number of attractive features with respect to conventional photovoltaic-silicon based cells (O'Regan and Grätzel, 1991; Tributsch, 2004; Cao et al., 2009; Chen et al., 2009; Yu et al., 2010; Yella et al., 2011; Bisquert et al., 2004; Gao et al., 2008; Ito et al., 2011; Grätzel and Zakeeruddin, 2013; Yum et al., 2012; Dwivedi et al., 2013): *(i)* low production/investment costs (easily to be produced by conventional roll-printing techniques); *(ii)* current devices are lightweight, semi-flexible and semi-transparent offering a variety of design opportunities not applicable to glass-based technologies (Hagfeldt et al., 2010); *(iii)* enhanced performance under real outdoor (bifacial cells capture light from all angles) and under higher temperatures conditions; *(iv)* highly operative under low or diffuse light (cloudy skies, indoor and even underwater conditions) (Li et al., 2019); *(v)* short energy payback time (<1 year); *(vi)* Although its relatively low solar energy conversion efficiency (up to ∼12%–13%) (Gratzel, 2009; Mathew et al., 2014),[4] when comparing with the best purchasable thin-film cells (up to 20%) (Grätzel and Zakeeruddin, 2013; Nazeeruddin et al., 2011), a better price/performance ratio can still be achieved allowing DSSCs to compete with other technologies.

Modern devices are composed of nano-porous layer of a semiconductor material (typically anatase-based TiO_2 nanoparticles), covered with a molecular dye (mostly based on Ruthenium complexes) (Hagfeldt et al., 2010) capable to harvest the incident sunlight mimicking the chlorophyll in green leave, immersed under an electrolyte solution above which is placed a platinum-based catalyst (cathode) (Govindaraj et al., 2015). It has been estimated that either Ru(II)-based or other organic dyes contribute to 10%–15% to the total costs of a DSSC, mainly due to costly synthesis (Hagfeldt et al., 2010). The search for alternative and more economic photosensitizes (dyes) may certainly contribute to further reduce its manufacturing costs.

Although DSSCs based on natural dyes show even lower efficiency values (0.1%–3%) (Hagfeldt et al., 2010; Li et al., 2019; Calogero et al., 2012, 2018; Shalini et al., 2015; Hao et al., 2006; Wongcharee et al., 2007; Yamazaki et al., 2007; Enciso and Cerdá, 2016; Enciso et al., 2017; Calogero and Marco, 2008; Meng et al., 2008; Zhang et al., 2008; Zhou et al., 2011; Hug et al., 2014; Castillo et al., 2016; Teoli et al., 2016; Lucioli et al., 2018; Guzel et al., 2018) than those made of synthetic pigments (up to ∼12% and ∼8% for Ru(II)-complexes and organic dyes, respectively) (Hagfeldt et al., 2010), the extremely low manufacturing and/or extraction costs make natural pigments a competitive alternative. The costs for natural dyes are quite difficult to estimate and mainly depend on the availability of the source and the extraction method. However, the use of cheap sources or waste streams of the food industry can be a good option. In this regard, pigments extracted from algae represent an attractive alternative. More than 30 million tons of seaweed are annually produced for industrial purposes and part of this production (*c.a.* 14 million tons) is composed of a few red seaweed species used for hydrocolloid (agar and carrageenan) extraction (FAO, 2018). Biorefinery approach has been proposed (Siller-Sánchez et al., 2019) to recover valuable products from this biomass, including phycobiliproteins (Radmer, 1996) and simultaneously minimizing the solid wastes.

Among all the phycobiliproteins (Enciso and Cerdá, 2016), the water-soluble light-harvesting phycoerythrin proteins found in cyanobacteria, red algae and cryptophytes, have some unique characteristics that make this protein a good candidate as a primary pigment (Li et al., 2019; Enciso and Cerdá, 2016; Enciso et al., 2018): *(i)* R-phycoerythrin (**R-PE**) is quite a stable 240 kDa protein formed by a basic $\alpha\beta$ heterodimer, that oligomerize to $(\alpha\beta)_6$ hexamer organized in an annular architecture, like all phycobiliproteins (Jiang et al., 1999; Sepúlveda-Ugarte et al., 2011). *(ii)* Each α subunit contains 2 phycoerythrobilin (PEB) chromophores whereas each β subunit contains two PEB and one phycourobilin (PUB). Both, PEB and PUB are open-chain tetrapyrrole chromophores covalently linked to specific cysteine residues of the apoprotein by a thioester linkage (Scheme 1) (Sepúlveda-Ugarte et al., 2011; Contreras-Martel et al., 2001; Vásquez-Suárez et al., 2018). Such a high number of chromophores (34 chromophore per **R-PE** molecule), sensing different environments, contributes to a broad absorption spectrum in the visible region of the electromagnetic spectra (450–600 nm) with an exceptionally high absorption coefficients, ε, at the maximum centred at *ca.* 550 nm (ranging from 1.81×10^6 M^{-1} to cm^{-1} 2.1×10^6 M^{-1} cm^{-1}, according to different authors) (Sepúlveda-Ugarte et al., 2011; Glazer and Stryer, 1984). *(iii)* **R-PE** provides quite a broad pH-operational range since this protein shows to remarkable functional stability in the pH range of 3.5–10.0 (Liu et al., 2009). *(iv)* The presence of free carboxylic acid groups can contribute to better anchor the protein on the surface of the semiconductor. This is a crucial step to assure the electron flow in the cell (Hagfeldt et al., 2010; Enciso and Cerdá, 2016; Enciso et al., 2018, 2016).

In addition, the use of additives that can expand the overall absorption spectrum and/or to decrease the UV-ageing phenomena can certainly improve the efficiency as well as the stability of operating DSSCs (Hagfeldt et al., 2010). In this context, β-carbolines (βCs) (Scheme 1) represent a group of alkaloids having quite interesting intrinsic photophysical and photochemical properties, that deserve to be investigated. Briefly, βCs show an extremely high photochemical stability, a relative low efficiency of photoinduced reactive oxygen species generation, quite large absorption coefficients (ε) in the UVB/UVA region (∼2.5×10^4 M^{-1} cm^{-1} and ∼5×10^3 M^{-1} cm^{-1}, respectively), high quantum yields of fluorescence in the visible region ($0.4 < \Phi_F < 0.98$) as well as excellent antioxidant properties (Mercader et al., 2009; Gonzalez et al., 2009a,b; Cabrerizo et al., 2010; Hrsak et al., 2015; Rasse-Suriani et al., 2018, 2016). Thus, the use of βCs can have several ramifications: *(i)* acting as a secondary pigment harvesting UVA light *(ii)* having a direct impact on the stabilization of the protein (both either improving or affecting protein stability towards denaturation); *(iii)* stabilizing the protein anchorage to the electrode surface; and/or *(iv)* affecting the redox behaviour of **R-PE**, all factors with great influence on cell performance.
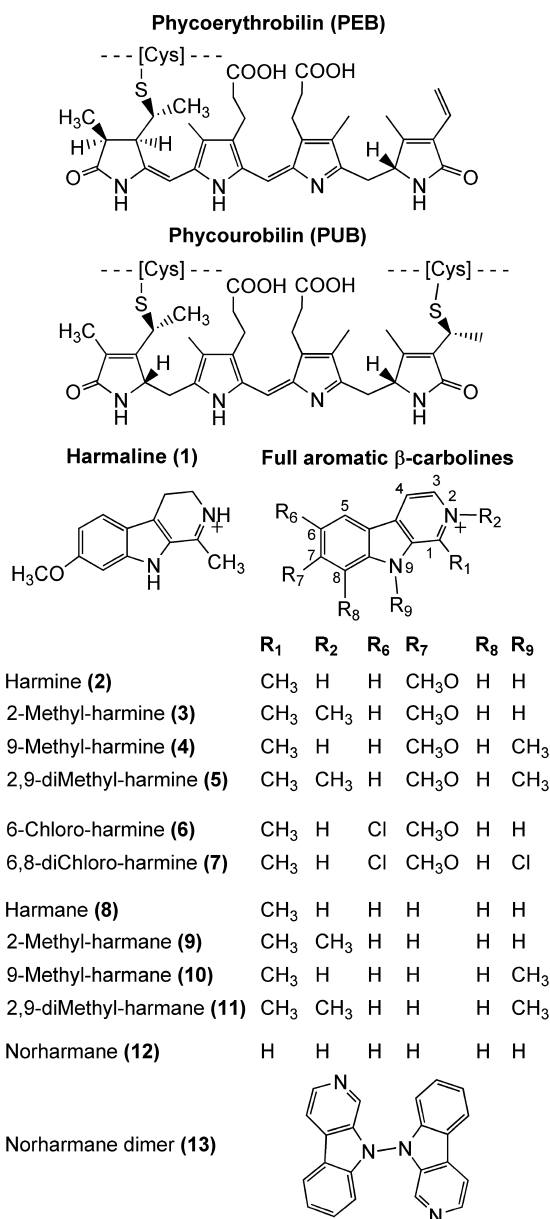
In this work, the red protein **R-PE**, extracted from two different algae species *Anotrichium furcellatum* and *Palmaria decipiens*, was evaluated as photosensitizer in DSSCs, in combination with a set of UVA absorbing chromophores derived from the βC family. We propose herein a fundamental electrochemical and spectroscopic complementary study on all the investigated compounds to further understand and elucidate the best operative conditions for a DSSC base on **R-PE** natural pigment.

2. Materials and methods

2.1. Chemicals and procedures

MilliQ water and reagent grade chemicals were used without further treatment. β-carboline (βCs) harmine (**2**), Harmaline (**1**) and Harmane (**8**) were provided by Sigma-Aldrich and were used without further purification. Methyl- and chloro-βC derivatives

---

[4] Highest certified solar-to-electric power conversion efficiencies reported varies according to the chemical structure of the dye, the electrolyte and the semiconductor. To date, the most efficient DSSC made of a single absorber component (photosensitizer) based on ruthenium (II)-containing metallorganic dyes adsorbed on nanocrystalline TiO_2, in conjunction with iodide-based electrolytes, achieved a certified efficiency of 11.9% under full sun illumination (AM 1.5 G, 1, 000 W m-2). Gratzel (2009) On the other hand, DSSC based on porphyrin derivatives using the cobalt(II/III) redox shuttle exhibit power conversion efficiencies of 13%. Mathew et al. (2014).

Phycoerythrobilin (PEB)

Phycourobilin (PUB)

Harmaline (1)   **Full aromatic β-carbolines**

	R_1	R_2	R_6	R_7	R_8	R_9
Harmine (2)	CH_3	H	H	CH_3O	H	H
2-Methyl-harmine (3)	CH_3	CH_3	H	CH_3O	H	H
9-Methyl-harmine (4)	CH_3	H	H	CH_3O	H	CH_3
2,9-diMethyl-harmine (5)	CH_3	CH_3	H	CH_3O	H	CH_3
6-Chloro-harmine (6)	CH_3	H	Cl	CH_3O	H	H
6,8-diChloro-harmine (7)	CH_3	H	Cl	CH_3O	H	Cl
Harmane (8)	CH_3	H	H	H	H	H
2-Methyl-harmane (9)	CH_3	CH_3	H	H	H	H
9-Methyl-harmane (10)	CH_3	H	H	H	H	CH_3
2,9-diMethyl-harmane (11)	CH_3	CH_3	H	H	H	CH_3
Norharmane (12)	H	H	H	H	H	H

Norharmane dimer (13)

Scheme 1. Chemical structure of the compounds investigated herein.

as well as N(9)-N(9')-nHo dimer ((nHo)$_2$) were synthesized following the procedures described elsewhere (Rasse-Suriani et al., 2018, 2016; Erra-Balsells and Frasca, 1983).

R-Phycoerythrin (**R-PE**) was extracted from *Anotrichium furcellatum* and *Palmaria decipiens*. *A furcellatum* was collected from Puerto Madryn (Argentina) in July 2017 by SCUBA diving at a hard 3 m depth-bottom (42°47′13.03″ S, 64°56′57.07″ W). At laboratory, the taxonomic identity of biological samples was confirmed before inspection under 100 to 400X magnification. Tissues were cleaned of epibionts and other debris in seawater, briefly washed consecutively with tap water and ethanol 96%, and dried to constant weight at 40 °C. *P. decipiens* was collected in January at seaside shores of the Antartic area (62°09′31, 1″ S, 58°56′29.8″ W), briefly washed with tap water followed by Milli-Q water at the laboratory, dried under hot air and then stored at 4 °C.

R-PE extraction and purification was done following the procedure described elsewhere (Enciso et al., 2018) giving **R-PE**

(raw) and **R-PE (pure)** samples. Final pH values (2.0, 3.0, 5.0 or 6.8) were adjusted adding microdrops of concentrated H_2SO_4 or using phosphate buffer solutions. An absorption coefficient ($\varepsilon^{550 \, nm}$) value of 1.96×10^6 M^{-1} cm^{-1}, at the 550 nm, was used to further calculate the concentration of **R-PE** solutions.

2.2. Techniques and equipment

Spectro-electrochemistry. Electrochemical experiments were carried out with a Dropsens-SPELEC spectro-electrochemical equipment coupled with screen printed gold electrodes (Dropsens C110 and AUTR10). Voltammograms were recorded in air-equilibrated conditions. In milliQ-aqueous media, phosphate buffer (0.1 M, pH 6.8) or NaClO$_4$ (0.1 M) were used as supporting electrolytes. The pH of non-buffered solutions was adjusted to 2.0, 3.0 and 5.0 by adding, when necessary microdrops of H$_2$SO$_4$ (3 M). The potential of the pseudo reference electrode in water solutions was 0.228 V vs. SHE. The latter value was determined by adding the redox couple ferricyanide/ferrocyanide (E = 0.358 V vs. SHE). In the case of the experiments performed in acetonitrile (MeCN), tetraethylammonium perchlorate (0.04 M) was used as supporting electrolyte. In this case the potential of the pseudo reference electrode was 0.347 V vs. SHE. The latter value was determined by adding the redox couple ferrocene/ferrocenium (E = 0.640 V vs. SHE). Voltammetric profiles obtained for supporting electrolytes under each condition are shown in Fig. SI.1. For comparative porpoises, the potential values reported herein were corrected and depicted vs. Ag/AgCl. *In situ* UV–visible absorption spectra were recorded using screen-printed gold optically transparent electrodes on a plastic substrate (DRP-AUTR10).

UV–visible absorption spectroscopy. UV–visible spectra of fresh solutions were obtained in a spectrophotometer Lambda 25 (Perkin Elmer). Each spectrum was acquired in the range within 200 and 800 nm with a resolution of 1 nm. A quartz cell with an optical pathway of 1 cm was employed for the experiments (Rasse-Suriani et al., 2018, 2016). The concentration of **R-PE** solutions was calculated according to Beer–Lambert's equation using a molar absorption coefficient value at 550 nm, $\varepsilon^{550 \, nm}$ of 1.96×10^6 M^{-1} cm^{-1}.

Fluorescence Excitation–Emission spectroscopy. The acquisition of fluorescence excitation–emission matrixes was performed in a spectrofluorometer Fluoromax4 (HORIBA Jobin Yvon) (Rasse-Suriani et al., 2018). The instrument consists in a Xenon lamp, two monochromators-excitation and emission, respectively- and a photomultiplier R928. The data was processed using a PC with the FluorEssence™ software. Matrixes were acquired scanning the emission within the range 250 y 600 nm with a resolution of 5 nm while recording the excitation spectrum in the range between 296 and 700 nm with a resolution of 2 nm.

2.3. DSSCs assembly and characterization

For DSSCs, FTO/TiO$_2$ electrodes (DYESOL, screen printed with Dyesol's DSL 18NR-AO Active Opaque Titania paste, active area of 0.7 cm^2) and FTO/Pt (screen printed with SOLARONIX's Pt Platinum Catalyst) were used as working and counter electrodes. The selected electrolyte was 50 mM iodide/tri-iodide (I$^-$/I$_3^-$) in acetonitrile (SOLARONIX Iodolyte AN-50) 30. When βC alkaloids were evaluated as additives three different procedures were followed for DSSCs assembly and preparation: *(i)* a βC solution was prepared and directly added to the FTO/TiO$_2$ electrode surface free of **R-PE**; *(ii)* a mixture of **R-PE** and βCs was prepared and added to the FTO/TiO$_2$ electrode surface; and *(iii)* the photoelectrode was incubated first with the **R-PE** solution and after 24 h the electrode was rinsed and then the βCs dissolved in water was added to the photoelectrode surface.

Current density vs. voltage (J-V) and electrochemical impedance spectroscopy (EIS) were measured on assembled DSSCs with a CHI 604E potentiostat. J-V characterizations were accomplished at a potential scan rate (v) of 0.05 Vs^{-1}, at room temperature, in the dark and under illumination (100 mW cm^{-2}) using a solar simulator from (ABET Technologies, 1 sun, 1.5 AM). On the other side, EIS experiments were carried out at potentials between 0 and 0.65 V measuring within the frequency range 0.1 Hz to 3 MHz (in the dark and under illumination).

3. Results and discussions

3.1. Electrochemical characterization of βCs

Four representative groups of βC derivatives were studied by cyclic voltammetry. These compounds were selected taking into account their intrinsic physicochemical and photochemical properties in connection with the processes involved in DSSCs: *(i)* harmine derivatives, due to their higher capability to participate in photo-redox processes; *(ii)* harmane derivatives, a group of photo-stable compounds with a distinctive ground and photoexcited electronic distribution, showing quite a high intrinsic fluorescence efficiency in the visible region; *(iii)* N-methyl- and *(iv)* chloro-derivatives as representative examples of electron rich and deficient βC-aromatic ring, respectively; and *(v)* harmaline (**1**), as representative example of 3,4-dihydro-βC derivatives with a distinctive redox activity and a relatively large absorption coefficient in the visible region of the electromagnetic spectra.

Voltammetric profiles were registered in air-equilibrated solutions, using gold electrodes and 0.1 M NaClO$_4$ (pH 3) as supporting electrolyte, following different potential scan rates and routines. It is worth mentioning that, under these conditions, all evaluated compounds showed adsorption to the electrode surface. This is accounted by the decrease in the cathodic peak related to the O-desorption, *c.a.* 0.60 V. The latter effect was particularly notorious for the cationic βCs. When applying very negative electrode potentials, the gold surface become clean and compounds are desorbed.

In the cases of full-aromatic βCs having no substituent at N(2) (*i.e.* **2**, **4**, **6**, **7**, **8**, **10** and **12**), voltammograms recorded either at $v = 0.05$ V s^{-1} (Figs. 1 and SI.2) or 0.01 V s^{-1} (Fig. SI.3) exhibited two well defined anodic contributions at *c.a.* 0.9 V and *c.a.* 1.2 V vs Ag/AgCl (Table 1). Their respective redox couples are clearly defined when using acetonitrile as solvent (Fig. SI.4 and Table 1). Although these seven compounds showed the same profile, it is worth to mention that the relative intensity of the first oxidation peak (*ca.* 0.9 V) shown by **2**, **4** and **10** is considerably higher than that observed for **6**, **7**, **8** and **12**. A similar effect was previously reported by Allen and Powell (1958) for related compounds and this phenomenon was attributed to the presence of a methoxy group as substituent in the aromatic ring.[5] Instead, our data support the hypothesis that this effect is closely related to the intrinsic capability of each substituent to further increase or decrease the overall electronic density of the aromatic βC ring. This is accounted by the fact that compounds lacking the methoxy substituent (such as **10**) also show a relatively high intensity of the first oxidation peak. On the other hand, chloro-derivatives **6** and **7** that contain the methoxy group show lower intensities than **1**. For cationic derivatives (**3**, **5**, **9** and **11**) voltammograms recorded at $v = 0.05$ V s^{-1} showed one broad oxidation peak at *c.a.* 1.10 V suggesting the presence of two overlapped electrochemical processes (Table 1 and Figs. 1b and SI.2). This is confirmed by the presence of two well defined peaks observed on voltammograms recorded at lower scan rates, $v = 0.005$ V s^{-1} (Fig. 1b, *inset*). It is noteworthy that methyl substituent placed at N(2) induces a large shift towards more positive potential values. In turn, voltammogram of the dihydroβC investigated, **1**, showed four oxidation peaks (Table 1 and Fig. 1). The two peaks observed at higher oxidation potentials were coincident with those shown by **2**.

Results presented herein are in line with the general mechanism proposed by Agüí et al. (2007) for compounds **1**, **2** and **8**, where the dihydro-derivative (**1**) follows a two-electron oxidation process giving rise to the formation of the corresponding full-aromatic derivative (*i.e.*, **2**). Full-aromatic βC ring can be further oxidized following another two-electrons oxidation process Agüí et al. (2007), Stanković et al. (2015), Švorc et al. (2015). However, we demonstrate herein for the first time that each of these two oxidation processes occur in two consecutive one-electron steps as is depicted in Scheme 2. The latter difference might be accounted for by the different experimental conditions used (electrode, pH and/or solvent conditions).

---

[5] Authors stated that the methoxy group could induce a particular stabilization for the cationic intermediate species formed upon oxidation with the concomitant reorganization with the solvent.
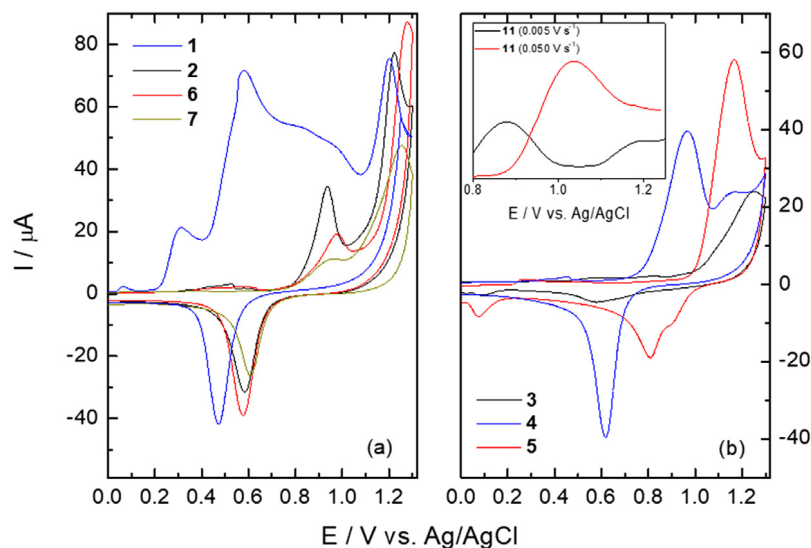

Fig. 1. Voltammetric profiles for screen printed Au-*pc* of **(a)** chloro-harmine and **(b)** N-methyl-harmine derivatives in 0.1 M NaClO$_4$ (pH 3.0) aqueous solutions, at $v = 0.050$ V s^{-1} and room temperature. *Inset*: compound **11** in 0.1 M NaClO$_4$ (pH 3.0) aqueous solutions ($v = 0.005$ V s^{-1} and 0.05 V s^{-1}).

Table 1
List of peak oxidation potential (E_{ox}) of βC derivatives measured in NaClO$_4$ (0.1 M) acidic aqueous and acetonitrile (MeCN) solution, at $v = 0.050$ V s^{-1} and room temperature.

Compound	pH	$E_{ox}^{(Water)}$/V	$^a E_{ox}^{(MeCN)}$/V
1	3.0	0.31, 0.58, 0.96 and 1.20	
	5.0	0.17, 0.66, 1.00 and 1.25	
2	3.0	0.94 and 1.22	($E_{an} = 1.05$; $E_{cat} = 0.75$) and ($E_{an} = 1.40$; $E_{cat} = 1.07$)
	3.0	*(0.50, 0.94, 1.05 and 1.22)	
	5.0	0.93 and 1.12	
3	3.0	1.22	
	3.0	*(0.95 and 1.18)	
	6.8	^{c}1.03 and ^{c} 1.17	
4	3.0	0.93 and 1.18	($E_{an} = 1.18$; $E_{cat} = 0.90$) and ($E_{an} = 1.40$; $E_{cat} = 1.27$)
	3.0	*(0.93 and 1.18)	
5	3.0	1.16	
	3.0	*(0.91 and 1.20)	
6	2.0	^{b}0.93 and ^{b}1.17	($E_{an} = 0.90$; $E_{cat} = $ nd) and ($E_{an} = 1.20$; $E_{cat} = $ nd)
	3.0	0.98 and 1.27	
	5.0	^{b}0.95 and 1.21	
	6.8	^{c}0.92 and ^{c}1.28	
7	3.0	0.95 and 1.27	($E_{an} = 0.95$; $E_{cat} = 0.60$) and ($E_{an} = 1.23$; $E_{cat} = 1.19$)
	6.8	^{c}0.96 and ^{c}1.24	
8	3.0	0.93 and 1.21	
	3.0	*(0.60 and 1.27)	
9	3.0	1.20	
	3.0	*(0.93 and 1.15)	
10	3.0	0.93 and 1.25	($E_{an} = 0.90$; $E_{cat} = 0.62$) and ($E_{an} = 1.38$; $E_{cat} = 1.10$)
	3.0	*(0.93 and 1.25)	
11	3.0	1.16	
	3.0	*(0.92 and 1.24)	
12	3.0	0.90 and 1.33	
	3.0	*(0.91 and 1.30)	
13	3.0	0.92 and 1.29	
R-PE (pure)	3.0	0.90	
	5.0	0.98	
	6.8	1.10	
R-PE (raw)	5.0	^{d}0.90 and 0.98	
R-PE + 3	6.8	^{c}0.70	
R-PE + 6	2.0	^{b}1.0	
	5.0	^{b}1.1	
	6.8	^{c}0.80	
R-PE + 7	6.8	^{c} 1.02	

*Peak-values observed in the voltammograms recorded after 500 repeated cycles between 1.0 and 1.2 V.
^{a}These oxidation potentials are corrected and referred vs. Ag/AgCl, as in aqueous media.
^{b}Values obtained from the deconvoluted signal shown in Fig. 5.
^{c}Values obtained from the deconvoluted signal shown in Fig. SI.7.
^{d}Values ascribed to chlorophyll. Nd = not detected.

The effect of pH was qualitatively investigated by measuring the voltammogram in pH 5.0 aqueous solutions of **1** and **2**, as representative examples of dihydro- and full-aromatic derivatives, respectively (Fig. 2). Briefly, voltammograms recorded at pH 5.0 for the full aromatic derivatives showed, under both high and low scan rates (0.05 V s^{-1} and 0.01 V s^{-1}), the two oxidation peaks described in the experiments performed at pH 3 (Fig. 1). On the contrary, in the case of **1**, results show that the number and position of the oxidation peaks depend on both the pH and the potential scan rate. Briefly, at pH 5 and at high scan rate (0.05 V s^{-1}), although the four peaks described at pH 3.0 were also observed, a shift on the oxidation potential was clearly detected on the first two peaks (Table 1). In contrast, under low potential scan rate (0.01 V s^{-1} and pH 5.0) these peaks were not detected. This fact suggests that the kinetic of the process connected to these two peaks are favoured under higher acidic conditions (pH < 3.0).

3.2. Spectro-electrochemical characterization of the oxidation products

It has been widely accepted that βC radical-cation produced upon electrochemical oxidation would follow a thermal reaction giving rise to the formation of symmetric βC dimers ((βC)$_2$) (Agüí et al., 2007). However, the data reported are not as convincing as one might otherwise desire and direct evidence of dimerization have not been reported to date. Moreover, in the case of N-methyl-derivatives the presence of the methyl group would reduce or avoid due to steric effects) the efficiency of such a dimerization process.

To begin with, the fate of the cationic species produced on the electrode surface from βC solutions was investigated. Briefly, after being subject to highly oxidative conditions (i.e., under 500 repeated cycles between 1.0 and 1.2 V) voltammogram profiles were recorded for all the investigated compounds (Fig. SI.5). All
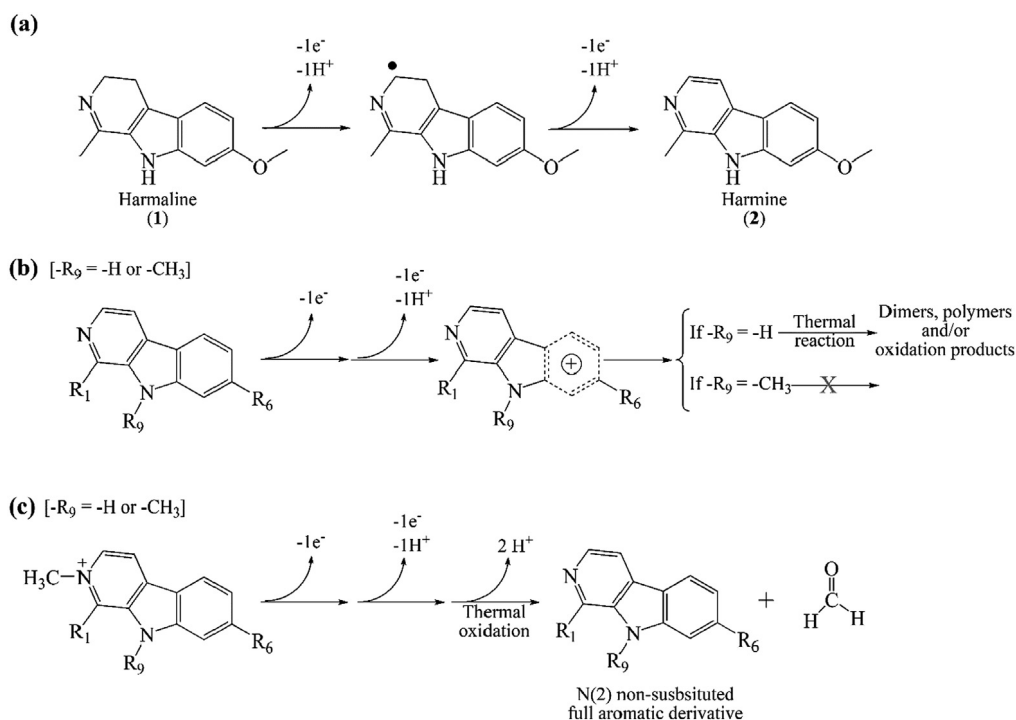
Scheme 2. Proposed oxidation mechanism of: **(a)** harmaline as a representative example of dihydro-derivatives, and **(b)** and **(c)** N(2) non-substituted and cationic N(2)-substituted full-aromatic βCs, respectively.
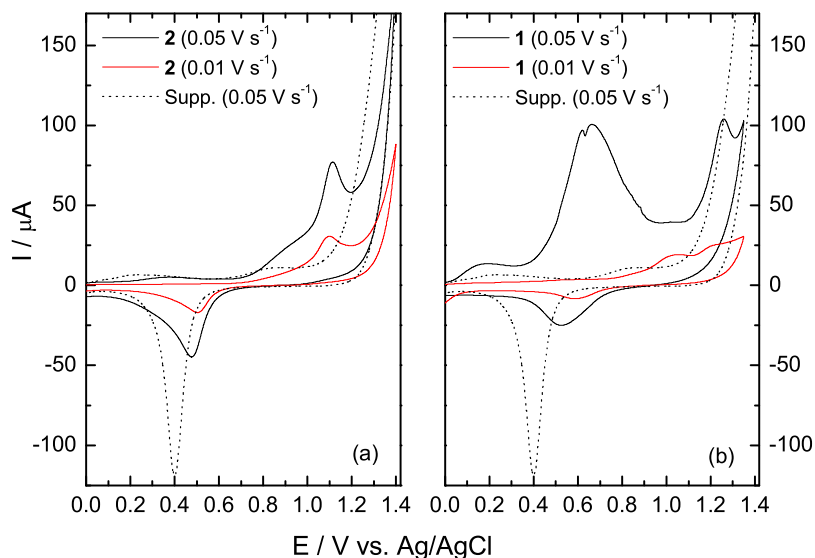

Fig. 2. Voltammetric profiles for screen printed Au-*pc* of **(a)** **2** and **(b)** **1** in 0.1 M NaClO$_4$ (pH 5.0) aqueous solutions, at two different potential scan rates ($v = 0.010$ V s^{-1} and 0.050 V s^{-1}) and room temperature. For comparative porpoise, supporting electrolyte profile (pH 5.0, $v = 0.050$ V s^{-1}) is included.

9-methyl derivatives were stable (Scheme 2b). Instead, unsubstituted βCs and cationic N(2)-methyl-derivatives showed a thermal reorganization of the electrochemically induced cation, giving rise to the formation of new products (Fig. SI.5 and Table 1). Surprisingly, in the cases of N(2)-methyl-derivatives, the new anodic contributions observed in the voltammograms appear placed at the same position of the peaks corresponding to their respective N(2)-unsubstituted-full aromatic βC derivative (Scheme 2c).

To further investigate the fate of the cation electrochemically formed from unsubstituted βCs UV–visible absorption spectra of **12** and **10** were recorded using screen printed transparent electrodes, during the application of different electrochemical routines. These two particular βCs were selected having in mind that,

in the case of **12**, the lack of substituents in the βC-ring would allow the formation of stable symmetric dimers (**13**). On the contrary, the presence of two methyl groups at C(1) and N(9) in **10** would give place to an steric impediment decreasing the chances of symmetric dimerization. For comparative purpose, the UV–visible spectrum (Fig. 3a) and the corresponding voltammogram (Fig. SI.2) of **13** standard solution were also recorded.

Briefly, the spectra of the three βCs recorded prior to oxidation showed two absorption bands in the spectral range between 300 nm and 450 nm (Fig. 3). These spectra can be interpreted as a combination of the absorption spectra of the corresponding protonated (βCH$^+$) and neutral (βCN) species (Fig. SI.6) (Rasse-Suriani et al., 2018, 2016). The fact that the neutral species is

adsorbed and detected even under highly acidic conditions (pH 3) suggests that the electrode surface plays a key role in the displacement of the βC acid base equilibria towards the neutral species (Scheme 2).

Under oxidative conditions (*i. e*, under the application of potential cycles in the range 1.0 V–1.2 V during 30 min) the UV–visible absorption spectra of oxidized **12** and **10** showed changes giving rise to a βC-like chromophore (see red lines in Fig. 3). Typically, the broad and intense band of the βCs centred at *ca.* 370–380 nm follows a relative decrease towards a relative increase in the intensity of the band centred at *ca.* 320 nm. These spectra show similarities when comparing with that recorded for the symmetric dimer **13** (Fig. 3a). Thus, at least for **12**, dimerization may be taking place during the thermal reorganization of the cation radicals generated in the surface of the electrodes at high positive potential values. These results show, for the first time, direct spectroscopic evidence regarding the latter process. It is noteworthy that, when subject to oxidative cycles, **2** and **8** give rise to the formation of a peak centred at *ca.* 0.5 V rather frequent for full-aromatic βCs. Thus, the presence of the methyl group at C(1) and/or the methoxy group at C(7) would play a negative role in the dimerization process, giving rise to the formation of other products. To further support the hypothesis stated in this paragraph potentiostatic experiments in addition to mass spectrometry as well as other spectroscopic techniques are needed.

3.3. Electrochemical and spectroscopic characterization of **R-PE**

Although **R-PE** is a widely studied and characterized protein its electrochemical properties still remains unknown. To begin with, voltammograms for raw and pure **R-PE** were recorded and the pH-effect was evaluated (Fig. 4a). Briefly, the peak potential value related to oxidation of the protein placed at *ca.* 1.0 V is pH dependent (Table 1). In addition, voltammograms recorded from raw material show an extra peak at 0.90 V, assigned to the presence of a very small fraction of chlorophyll. This is also confirmed by the appearance of weak absorption (*ca.* 650 nm, Fig. 4b) and emission (*ca.* 660 nm, Fig. 4c, left column) bands.

Pigment composition in red algae is dominated by phycoerythrin (**R-PE**), phycocyanin (PC), allophycocyanin (APC) and chlorophyll *a* (Hurd et al., 2014). Interspecific differences in pigment balance are considered physiological adaptations to different light environments (Dring, 1981) and **R-PE** dominate in species adapted to deep waters (Dring, 1981; Pritchard et al., 2013). Intraspecific fluctuations are considered physiological adaptations to seasonal (Schmid et al., 2017; Pereira et al., 2012) and depth (Dring, 1981; Gómez et al., 2005) environmental variations. **R-PE** has been reported to be the dominant pigment of *P. decipiens* regardless of seasonal fluctuations (Lüder et al., 2001). Pigment composition of *A. furcellatum* has not been reported to our knowledge. However, related species *Anotrichium crinitum* and *Griffithsia pacifica* had been considered as deep-water species with a pigment composition also dominated by **R-PE** (Pritchard et al., 2013; Waaland et al., 1974). In this context, data reported herein in Fig. 4 suggest that, albeit present in the raw extracts, chlorophyll and other phycobiliproteins are in very low relative concentration or negligible with respect to **R-PE**.

In addition, raw extracts show the presence of a set of emitting indole-like chromophores (insets in Fig. 4c). However, the concentration of the latter compounds decreases substantially after purification. Other non-fluorescent secondary metabolites (such as carotenoids, carbohydrates, etc.) can also be removed after purification. These metabolites can play a key role in the overall DSSCs efficiency either acting as photosensitizers (Yamazaki et al., 2007; Hug et al., 2014) or as stabilizers of **R-PE** in solution (see Fig. 4).

3.4. Effect of βcs in the stability of **R-PE**

In order to explore the potential use of βC alkaloids as additives for **R-PE**-based DSSCs, the interaction between **R-PE** and βCs was investigated. 2-methyl-harmine (**3**) and the two chloroharmines (**6** and **7**) were selected as representative examples of electron rich and deficient βC-full aromatic rings, respectively (Fig. 5 and SI.7). The addition of these βCs into **R-PE (pure)** solution induces changes in the oxidation potential of the protein. *I. e.*, chloroharmines increase the oxidation potential, whereas methyl-derivative induces the opposite behaviour (Table 1). Changes are more evident in the respective deconvolution plots (*right column*). In particular, **6** affects the redox potential of **R-PE (pure)** in a dose-dependent manner: **R-PE** displayed an oxidation peak at 0.98 V, at pH 5.0, whereas after the addition of **6** the anodic peak ascribed to the protein moves to 1.1 V (Fig. 5). The other oxidation contribution arises from the βC itself. The same trend was observed when working at pH 2.0 and 6.8 (Fig. SI.7 and Table 1).

In operating DSSCs, sunlight passes through the transparent electrode into the dye layer. The photoexcited dye is oxidized as a consequence of the injection of one electron into the conduction band of the semiconductor. The injected electron migrates through the sintered particle network to be collected at the front side transparent conducting oxide (TCO) electrode. On the final step, the dye is restored by the electron donation from an electrolyte-redox system, typically the iodide/triiodide (I^-/I_3^-) couple (Govindaraj et al., 2015). Thus, from the thermodynamic point of view, the efficiency of a DSSC depends on four distinctive energy levels: the first excited (LUMO) and ground (HOMO) states of the photosensitizer, the Fermi level of the TiO$_2$ electrode and the redox potential of the electrolyte. The driving force for the reduction of the oxidized dye by the electrolyte species is, in particular, defined by two components: the redox potential for $I_2^{\bullet-}/I^-$ couple (0.80 V vs NHE in acetonitrile) (Govindaraj et al., 2015) and the oxidation potential (E_{ox}) of the dye (related to the HOMO energy). The regeneration of the photo-oxidized dye by I^- therefore requires a dye HOMO energy level positioned at least lower than +0.9 V vs. NHE in energy. As can be deduced, the driving force to regenerate the oxidized dye becomes more favourable when the oxidation potential E_{ox} increases. Therefore, the shift towards more positive **R-PE** oxidation potential observed in the presence of chloroharmines make them good candidates as additive for DSSC assembly.

3.5. Effect of pH and temperature on the R-PE tetrapyrrole chromophores

The stability of the photosensitizers used in DSSCs is also a key aspect that can have a direct impact on the overall efficiency of the photovoltaic cell. **R-PE** is a protein and, as such, its conformation structure and, in consequence, the surrounding or local environment of the photoactive chromophore can be modified under different experimental conditions (pH, temperature, etc.). In this context, the effect of pH on the electronic transition states of **R-PE (pure)** was evaluated herein using UV–visible absorption spectroscopy (Fig. 6a). Briefly, spectra recorded under neutral (data not shown) and low acidic pH conditions (pH 5.0) were identical, showing the well-known absorption peaks at 498, 540 and 565 nm. On the contrary, spectrum measured under denaturing pH (pH 2.0) was visibly different indicating that the chromophore in the protein is sensing a different environment. This is consistent with a denaturation of the protein when subject to the lowest pH condition.

The effect of the temperature on the stability of the protein's chromophore was also evaluated by monitoring the changes in
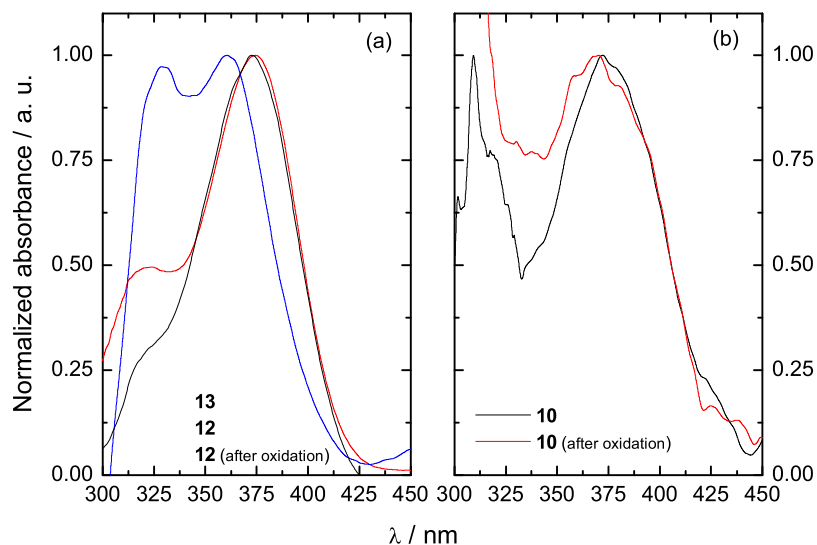
Fig. 3. UV–visible spectra recorded on transparent screen-printed Au-*pc* electrodes for: **(a) 12** after (black line) and before (red line) oxidation and **13** (blue line), and **(b) 10** after (black line) and before (red line) oxidation. (For interpretation of the references to colour in this figure legend, the reader is referred to the web version of this article.)
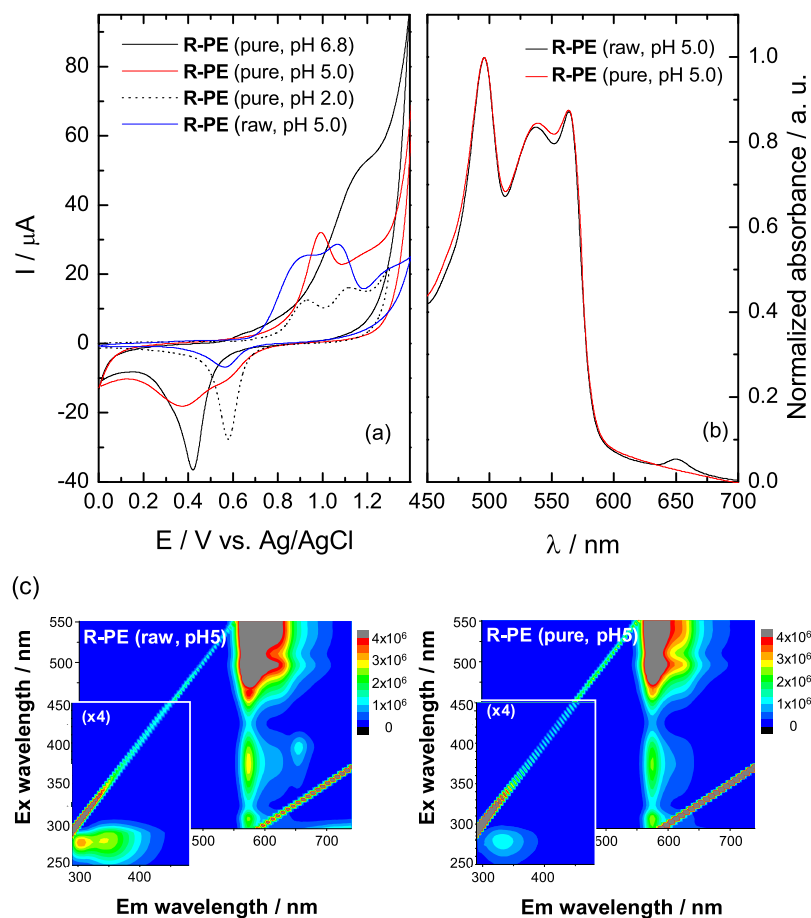

Fig. 4. (a) Voltammetric profiles for screen printed Au-*pc* in 0.1 M NaClO$_4$, at $v = 0.050$ Vs^{-1} and room temperature of raw and pure **R-PE** measured under different pH conditions. **(b)** UV–visible absorption and **(c)** fluorescence excitation–emission matrices recorded from raw and pure **R-PE** extracts solution at pH 5.0. *Insets* depict fluorescence matrices recorded at low excitation–emission range.

the absorbance at 565 nm ($A^{565\ nm}$)[6] of the protein solutions

subject to different temperatures. Transition temperature (T$_m$) value is a useful magnitude to quantitative account (compare) for the thermal stability of a given protein when subject to different
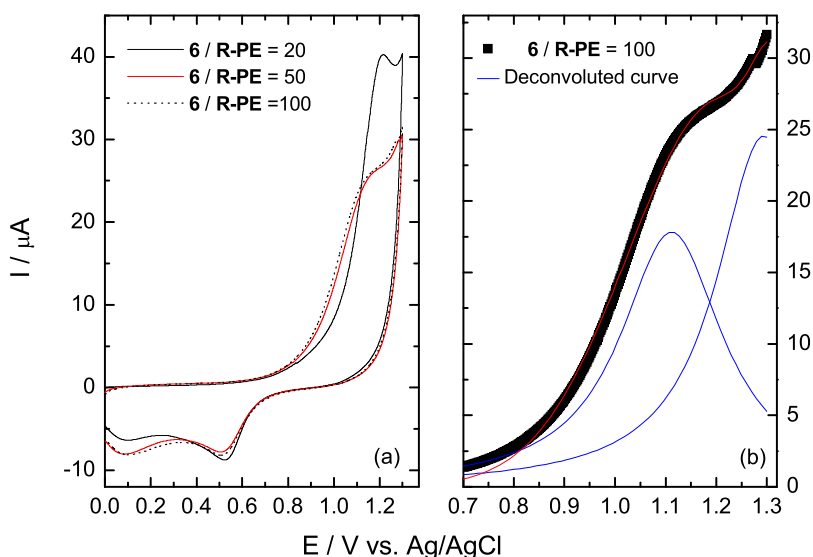
---

6 Authors stated that the methoxy group could induce a particular stabilization for the cationic intermediate species formed upon oxidation with the concomitant reorganization with the solvent.

Fig. 5. **(a)** Voltammetric profiles and **(b)** the corresponding deconvoluted peaks (*right column*) for screen printed Au-*pc* of **R-PE (pure)** (1 μM) in 0.1 M NaClO$_4$ measured in the presence of increasing amounts of **6** (20, 50 and 100 μM), at $v = 0.050$ Vs^{-1} and room temperature at pH 5.0.
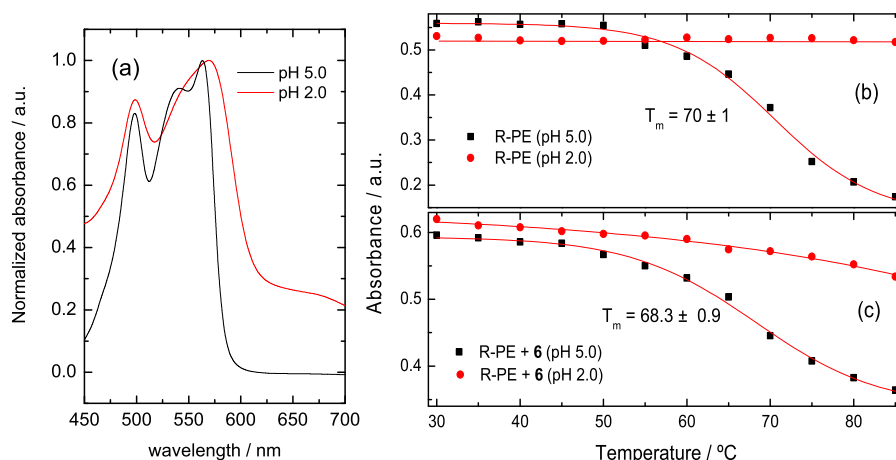

Fig. 6. **(a)** Normalized UV–visible absorption spectrum of **R-PE (pure)** in aqueous solution measured at pH 2.0 (red) and 5.0 (black). **(b)** and **(c)** show the dependence of $A^{565 \text{ nm}}$ with the temperature, measured from aqueous solutions of **R-PE (pure)** at pH 5.0 (black squares) and 2.0 (red circles) and a mixture of **R-PE (pure)** and **6** under same experimental conditions, respectively. (For interpretation of the references to colour in this figure legend, the reader is referred to the web version of this article.)

experimental conditions.[7] For each investigated system, T$_m$ value was obtained from the [**R-PE**] (or $A^{565 \text{ nm}}$ instead) *vs.* temperature plot (Fig. 6b and c). At pH 5.0, T$_m$ value obtained for **R-PE (pure)** was 70 ± 1 °C, suggesting a relative large operative temperature range for this protein. To further investigate whether the presence of βCs affect the stability of **R-PE**, the thermal effect was also evaluated in the presence of **6**. T$_m$ value obtained (68.3 ± 0.9 °C) was the same, within the experimental error, to that observed in the absence of the βC. Thus, the presence of the alkaloid neither prevent nor enhance the changes in the absorption capability of the protein induced by the temperature. On the contrary, under highly acidic pH conditions (pH 2.0), no further changes in the local environment of the protein's chromophore were observed (Fig. 6c) beyond the intrinsic changes induced by the pH (Fig. 6a). The chromophore in the denatured **R-PE** is sensing the same environment under the whole temperature range investigated.

Moreover, the addition of **6** slightly decreases the stability of the chromophore as is accounted for by the smooth decreased on $A^{565 \text{ nm}}$ as a function of the temperature (Fig. 6c).

3.6. Assembly and characterization of *R-PE* based DSSCs

DSSCs were assembled using FTO/TiO$_2$ photoanodes, sensitized by **R-PE** protein. The effect of the pH as well as protein purity on the DSSCs photovoltaic properties and their operating efficiency (η) were evaluated (Table 2). As representative examples, Fig. 7 and Table 3 depict electrochemical data (J$_{sc}$, V_{oc}, FF and η% efficiency) obtained for the higher [R-PR] tested under pH 2.0 and 5.0 conditions.

As expected, a dependence of the protein concentration ([**R-PE**]) on η was observed: the higher the number of incident photon absorbed by the chromophore, the higher the DSSC efficiency (Table 2). In addition, the efficiency of DSSCs measured after up to 22 days of being stored in the dark remained unchanged suggesting that DSSCs made of **R-PE** offer great stability.

Surprisingly, and despite the presence of a very small fraction of chlorophyll observed (Fig. 4), DSSCs assembled with raw
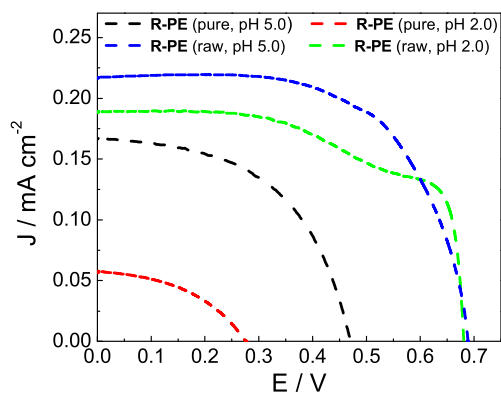
---

[7] According to the thermodynamic model, protein denaturalization equilibrium involves only two species: the protein in its native and denatured forms. Thus, Tm represents the temperature where the relative concentration of both fractions of the protein is the same.

Fig. 7. Representative photocurrent density–voltage (J–V) curves for the dye sensitized cells using pure and raw **R-PE** samples at pH 5.0 and pH 2.0.

Table 2
DSSCs efficiencies recorded under different experimental conditions. % error estimated was ± 0.003%.

	[R-PE]/μM	pH	η/%
R-PE (pure)	0.37	2.0	0.015, [a]0.022 and [b]0.022
			0.017 (+**6**, 74 μM)
		5.0	0.015
			0.009 (+**1**, 74 μM)
	0.61	2.0	0.026
			0.015 (+**6**, 74 μM)
	0.86	5.0	0.040
			0.024 (+**6**, 2.0 μM)
	3.4	2.0	0.007
		5.0	0.030
R-PE (raw)	0.37	2.0	0.020
		5.0	0.019
	0.61	5.0	0.031
			0.018 (+**6**, 74 μM)
		2.0	0.050
	0.86	5.0	0.073
			0.040 (+**3**, 25 μM)
	3.4	2.0	0.073
		5.0	0.110
βC	0	5.0	0.011 (+**6**, 150 μM)
		5.0	0.011 (+**1**, 460 μM)
		5.0	0.011 (+**2**, 290 μM)
MilliQ water(control)	0	2.0	0.011
		5.0	0.004

[a]Date measured after 2 days.
[b]Date measured after 22 days.

extracts yield higher η values (20%–30% of increase) than that based on **R-PE (pure)**. The lack of the previously described (Enciso et al., 2017) competitive effect of chlorophyll might be ascribed to the rather low relative concentration of the latter pigment with respect to **R-PE**, the dominant pigment present in *A. furcellatum* and *P. decipiens*. In addition, a small contribution of other phyco-biliproteins (PC and APC) (Pritchard et al., 2013; Waaland et al., 1974) can also have a cooperative effect (Li et al., 2019). A difference in the protein stability between pure and raw material could also account for the relative decrease in the efficiency observed. However, any difference was observed within these two extracts (data not shown). Thus, one can conclude that the presence of additional components (*i.e.*, proteins, polysaccharides and/or other secondary metabolites) (Hurd et al., 2014; Lynn Cornish and Garbary, 2010) present in the raw material might contribute to better anchoring **R-PE** to the semiconductor surface. Further studies are needed to fully address this hypothesis.

The pH can certainly affect the chemical nature of the pigment and, as such, the overall η of DSSCs (Teoli et al., 2016). To further evaluate this, DSSCs were assembled with dye solutions at two different pH conditions (2.0 and 5.0). These two pH conditions were chosen in order to evaluate whether the conformational structure of the protein affect the efficiency of the DSSCs. Results show that cell efficiencies observed under highly acidic conditions (pH 2.0) were up to 30%–50% lower (Table 2). Therefore, better DSSC yields would be observed when **R-PE** protein is present in its native form. This can be accounted for by the highest absorption coefficient as well as the smallest size (and, therefore, a better TiO$_2$ surface coating) shown by the native form of **R-PE**. In addition, it can be seen at a glance that the electrodes sensitized with **R-PE (raw)** at pH 5.0 exhibit the best colouration and a consequent superior performance (Fig. SI.8).

A transmission line-based model (Scheme SI.1) was successfully used to describe the electrochemical behaviour of DSSCs in the dark. Table 4 shows the values obtained after fitting the experimental results, where: R_{ct} is the charge transport resistance related to recombination of electrons at the TiO$_2$/dye/electrolyte interface; R_t is the electron transport resistance in the photo-anode; C_μ is the chemical capacitance at the TiO$_2$/dye/electrolyte interface, an equilibrium property that relates the variation of the electron density to the displacement of the Fermi level; $\Gamma_t = R_t \times C_\mu$ is the time constant for the transport of the injected electrons transported through the nanoparticle network and $\Gamma_{rec} = R_{ct} \times C_\mu$ is the recombination time that reflects the life-time of an electron in the photo-anode.

High recombination times are the main responsible for better efficiency performance. Especially when considering the ratio R_{ct} to R_t the impact could be better understood: a big ratio shows that electrons at the photoanode choose the path that involves the transference across the semiconductor towards the FTO/TiO$_2$ interface instead of choosing the recombination of the promoted electrons (after photoexcitation of the dye) with the triiodide couple of the electrolyte.

3.7. Effect of βCs as additive on DSSCs

Among all the βCs electrochemically characterized, the influence of three representative βCs on the η value of each cell was assessed. These particular βCs were chosen based on their intrinsic photophysical, photochemical and electrochemical properties. Briefly, photoexcited harmine (**2**) and its derivatives efficiently participate in electron transfer processes (Gonzalez et al., 2009a; Rasse-Suriani et al., 2016). The cationic N(2)-methyl derivative **3** induces a shift in the oxidation potential of **R-PE** towards more negative potential; whereas chloroharmine derivatives **6** and **7** showed the opposite effect (Fig. SI.7). In addition, **6** and **7** showed the highest antioxidant capabilities among all the investigated βC derivatives (Rasse-Suriani et al., 2016). Finally, compound **1**, was selected as a representative example of a βC that can efficiently absorbs the incident visible light (Scheme 1).

To get a reference point, DSSCs free of **R-PE** were firstly assembled with βCs (UVA-absorbing compounds) as a solely photosensitizer. The overall efficiency, η, observed was rather low and values similar for all the βCs investigated (Table 2). It is worth mentioning that the latter data were not corrected (normalized) by the total incident light. Thus, η values are not comparable with those obtained from DSSCs based on **R-PE**. Despite this, the

Table 3

Photovoltaic properties for DSSCs cells assembled using different sensitizers. All measurements were performed under a sun light intensity of 100 mW cm^{-2}, AM 1.5G and the active areas were 0.7 cm^2 for all the cells. J_{sc} is the current density, V_{oc} the open circuit potential, FF is the fill factor and η is the conversion efficiency. Results arise from at least three independent experiments performed for each dye ([R-PE] = 3.4 μM). These results can also be confirmed by impedance electrochemical spectroscopy measurements. The equivalent circuit used to these results is shown in Scheme SI.1.

	R-PE (raw)		R-PE (pure)		6	[a]R-PE (pure) + 6
	pH 5.0	pH 2.0	pH 5.0	pH 2.0	pH 5.0	pH 5.0
J_{sc}/A cm^{-2}	2.2×10^{-4}	1.9×10^{-4}	1.7×10^{-4}	5.7×10^{-5}	9×10^{-5}	1.4×10^{-4}
V_{oc}/V	0.69	0.68	0.47	0.27	0.31	0.40
FF	0.62	0.57	0.52	0.44	0.42	0.42
η/%	0.110	0.073	0.040	0.007	0.011	0.024

[a]Molar ratio βCs to R-PE equal to 3.

Table 4

Data calculated from measurements performed under dark conditions (at E = 0.5 V) fitted using the transmission line model.

	R-PE (raw)		R-PE (pure)		6	[a]R-PE (pure) + 6
	pH 5.0	pH 2.0	pH 5.0	pH 2.0	pH 5.0	pH 5.0
R_{ct}/Ω	418	271	335	177	295	452
R_t/Ω	13	15	10	8	17	16
$\Gamma_t = R_t \times C_\mu$/s	0.003	0.004	0.0015	0.0013	0.00016	0.0009
$\Gamma_{rec} = R_{ct} \times C_\mu$/s	0.09	0.07	0.05	0.03	0.003	0.02

[a]Measurements were performed at pH 5.0. Molar ratio βCs to R-PE equal to 3.

intrinsic electrochemical parameters (Γ_{rec} *ca.* 0.003 s and R_{ct}/R_t ratio *ca.* 18) for all DSSCs based on βCs were not as promising as one might desire (see representative data for compound **6** in Tables 2 and 3).

When βCs were tested as additives in DSSCs based on **R-PE**, a clear decrease on the efficiency of 50%–70% was observed for the four investigated compounds under both pH conditions (Table 2). This fact can be a consequence of conformational changes and/or deactivation of **R-PE** excited states induced by the βCs. However, these hypotheses are discarded on the bases of the lack of changes on both the absorption and fluorescence emission spectra (quenching) recorded in the presence of increasing amount of βCs (Fig. SI.9).

The decrease in the DSSC performance is better described by the electrochemical parameters obtained at 0.5 V listed in Tables 3 and 4. The use of βC (**6**) as additive leads to Γ_{rec} and R_{ct}/R_t ratio values lower than those observed for the best assembly represented by **R-PE** (raw, at pH 5.0) that shows Γ_{rec} and R_{ct}/R_t ratio values of 0.09 s and 32, respectively. When measuring at 0.45 V the R_{ct} to R_t ratio reaches the value of 100 for the case of the **R-PE** (raw, pH 5.0) showing a better electron transfer on the desired path. However, the addition of **6** to **R-PE (pure)** also leads to an improvement on the R_{ct} to R_t ratio. This fact suggests that βCs would have a positive role improving the coating of pure **R-PE** and the TiO$_2$ surface.

4. Conclusions

In this work, the electrochemistry of βC naturally occurring alkaloids and, in particular, the oxidative mechanism suggested for these compounds have been revisited. Data reported herein clearly suggest a more complex pattern of reaction directly related to the chemical structure of the βCs. Briefly, N(2) non-substituted βCs follow a two consecutive one-electron transfer steps, whereas the cationic βC derivatives show these oxidative steps at very high oxidation potentials with a concomitant thermal reorganization giving rise to the formation of the full aromatic N(2) non-substituted βCs. Moreover, the indolic nitrogen N(9) plays a key role in the thermal reorganization of the radical intermediate produced from N(2) non-substituted βCs when subject to high anodic potentials. In addition, the electrochemical properties of R-phycoerythrin (**R-PE**) red protein were addressed.

Finally, the photosensitizing properties of the investigated compounds were evaluated in DSSCs. The relatively high stability and intrinsic photo-electrochemical properties of **R-PE** make this protein an excellent candidate for DSSC assembly, reaching solar energy to electricity conversion efficiency values, η, up to 0.110%. In particular, the best efficiency was achieved by using raw extracts without further purification. This finding makes red algae an excellent source of natural pigments for DSSC devices. The cost- and time-effective extraction procedure would dramatically reduce the overall fabrication costs of DSSCs, rising-up the price/performance ratio. This may be particularly relevant in countries having a large phycocolloids industry based on the use of red algae where natural dyes can be obtained as side products.

On the other hand, despite their intrinsic properties make βCs good candidates as additive (co-photosensitizer), data reported herein showed that the addition of these alkaloids in operation DSSCs based on **R-PE** had a negative impact on the overall conversion efficiency. However, data suggest that βCs would play a role as UVB/UVA barrier. This might represent a potential advantage in the development of novel DSSCs in which this kind of UV-blocking agents can certainly increase the stability of the main pigment (**R-PE**) and, therefore, the DSSCs lifespan.

Declaration of competing interest

The authors declare that they have no known competing financial interests or personal relationships that could have appeared to influence the work reported in this paper.

- 3.3, respectively. F.M.C. thanks The World Academy of Science (TWAS) and TWAS-Young Affiliates Network (TYAN) for supporting the organization of the 1st TYAN International Thematic Workshop in photo-electrochemistry, held in Chascomús (Argentina).

Appendix A. Supplementary data

Supplementary material related to this article can be found online at https://doi.org/10.1016/j.egyr.2019.10.045.

References

Agüí, L., Peña Farfal, C., Yáñez Sedeño, P., Pingarrón, J.M., 2007. Electroanalysis 19, 237–243.

Allen, M.J., Powell, V.J., 1958. J. Electrochem. Soc. 105, 541–544.

Bisquert, J., Cahen, D., Hodes, G., Rühle, S., Zaban, A., 2004. J. Phys. Chem. B 108, 8106–8118.

Cabrerizo, F.M., Arnbjerg, J., Denofrio, M.P., Erra-Balsells, R., Ogilby, P.R., 2010. Chem. Phys. Chem. 11, 796–798.

Calogero, G., Barichello, J., Citro, I., Mariani, P., Vesce, L., Bartolotta, A., Di Carlo, A., Di Marco, G., 2018. Dye. Pigment. 155, 75–83.

Calogero, G., Marco, G.D., 2008. Sol. Energy Mater. Sol. Cells 92, 1341–1346.

Calogero, G., Yum, J.-H., Sinopoli, A., Di Marco, G., Grätzel, M., Nazeeruddin, M.K., 2012. Sol. Energy 86, 1563–1575.

Cao, Y., Bai, Y., Yu, Q., Cheng, Y., Liu, S., Shi, D., Gao, F., Wang, P., 2009. J. Phys. Chem. C 113, 6290–6297.

Castillo, D., Sanchez Jaurez, A., Espinosa Tapia, S., Guaman, A., Obrego Calderon, D., 2016. In: Kafafi, Z.H., Lane, P.A., Samuel, I.D.W. (Eds.), Organic Photovoltaics XVII. p. 9942.

Chen, C.-Y., Wang, M., Li, J.-Y., Pootrakulchote, N., Alibabaei, L., C.-h. Ngocle, Decoppet, J.-D., Tsai, J.-H., Grätzel, C., Wu, C.-G., Zakeeruddin, S.M., Grätzel, M., 2009. ACS Nano 3, 3103–3109.

Contreras-Martel, C., Martinez-Oyanedel, J., Bunster, M., Legrand, P., Piras, C., Vernede, X., Fontecilla-Camps, J.C., 2001. Acta Crystallogr. Sect. D 57, 52–60.

Dring, M.J., 1981. Limnol. Oceanogr. 26, 271–284.

Dwivedi, C., Dutta, V., Chandiran, A.K., Nazeeruddin, M.K., Grätzel, M., 2013. Energy Procedia 33, 223–227.

Enciso, P., Cerdá, M.F., 2016. Cold Reg. Sci. Technol. 126, 51–54.

Enciso, P., Decoppet, J.-D., Grätzel, M., Wörner, M., Cabrerizo, F.M., Cerdá, M.F., 2017. Spectrochim. Acta A 176, 91–98.

Enciso, P., Decoppet, J.D., Moehl, T., Gratzel, M., Worner, M., Cerda, M.F., 2016. Int. J. Electrochem. Sci. 11, 3604–3614.

Enciso, P., Woerner, M., Cerdá, M.F., 2018. MRS Adv. 3, 3557–3562.

Erra-Balsells, R., Frasca, A.R., 1983. Tetrahedron 39, 33–39.

FAO, 2018. The State of World Fisheries and Aquaculture - Meeting the sustainable development goals, Rome, Italy.

Gao, F., Wang, Y., Shi, D., Zhang, J., Wang, M., Jing, X., Humphry-Baker, R., Wang, P., Zakeeruddin, S.M., Grätzel, M., 2008. J. Am. Chem. Soc. 130, 10720–10728.

Glazer, A.N., Stryer, L., 1984. Trends Biochem. Sci. 9, 423–427.

Gómez, I., Figueroa, F.L., Huovinen, P., Ulloa, N., Morales, V., 2005. Aquaculture 244, 369–382.

Gonzalez, M.M., Arnbjerg, J., Paula Denofrio, M., Erra-Balsells, R., Ogilby, P.R., Cabrerizo, F.M., 2009a. J. Phys. Chem. A 113, 6648–6656.

Gonzalez, M.M., Salum, M.L., Gholipour, Y., Cabrerizo, F.M., Erra-Balsells, R., 2009b. Photochem. Photobiol. Sci. 8, 1139–1149.

Govindaraj, R., Senthil Pandian, M., Ramasamy, P., Mukhopadhayay, S., 2015. Bull. Mater. Sci. 38, 291–296.

Gratzel, M., 2009. Acc. Chem. Res. 42, 1788–1798.

Grätzel, C., Zakeeruddin, S.M., 2013. Mater. Today 16, 11–18.

Guzel, E., Arslan, B.S., Durmaz, V., Cesur, M., Tutar, O.F., Sari, T., Isleyen, M., Nebioglu, M., Sisman, I., 2018. Sol. Energy 173, 34–41.

Hagfeldt, A., Boschloo, G., Sun, L., Kloo, L., Pettersson, H., 2010. Chem. Rev. 110, 6595–6663.

Hao, S., Wu, J., Huang, Y., Lin, J., 2006. Sol. Energy 80, 209–214.

Hrsak, D., Holmegaard, L., Poulsen, A.S., List, N.H., Kongsted, J., Denofrio, M.P., Erra-Balsells, R., Cabrerizo, F.M., Christiansen, O., Ogilby, P.R., 2015. Phys. Chem. Chem. Phys. 17, 12090–12099.

Hug, H., Bader, M., Mair, P., Glatzel, T., 2014. Appl. Energy 115, 216–225.

Hurd, C.L., Harrison, P.J., Bischof, K., Lobban, C.S., 2014. Cambridge University Press, ISBN: 9781139948852, Release Date: July 17, 2014, Imprint: Cambridge University Press.

Ito, S., Dharmadasa, I.M., Tolan, G.J., Roberts, J.S., Hill, G., Miura, H., Yum, J.H., Pechy, P., Liska, P., Comte, P., Grätzel, M., 2011. Sol. Energy 85, 1220–1225.

Jiang, T., J.-p. Zhang, D.-c. Liang, 1999. Proteins 34, 224–231.

Li, W., Pu, Y., Ge, B., Wang, Y., Yu, D., Qin, S., 2019. Int. J. Hydrogen Energy 44, 1182–1191.

Liu, L.-N., Su, H.-N., Yan, S.-G., Shao, S.-M., Xie, B.-B., Chen, X.-L., Zhang, X.-Y., Zhou, B.-C., Zhang, Y.-Z., 2009. Bioenergetics 1787, 939–946.

Lucioli, S., Di Bari, C., Forni, C., Di Carlo, A., Barrajon-Catalan, E., Micol, V., Nota, P., Teoli, F., Matteocci, F., Frattarelli, A., Caboni, E., 2018. J. Photochem. Photobiol. B-Biol. 188, 69–76.

Lüder, U.H., Knoetzel, J., Wiencke, C., 2001. Polar Biol. 24, 598–603.

Lynn Cornish, M., Garbary, D.J., 2010. ALGAE 25, 155–171.

Mathew, S., Yella, A., Gao, P., Humphry-Baker, R., Curchod, B.F.E., Ashari-Astani, N., Tavernelli, I., Rothlisberger, U., Nazeeruddin, M.K., Grätzel, M., 2014. Nature Chem. 6, 242.

Meng, S., Ren, J., Kaxiras, E., 2008. Nano Lett. 8, 3266–3272.

Mercader, A.G., Duchowicz, P.R., Fernández, F.M., Castro, E.A., Cabrerizo, F.M., Thomas, A.H., 2009. J. Mol. Graph. Model. 28, 12–19.

Nazeeruddin, M.K., Baranoff, E., Grätzel, M., 2011. Sol. Energy 85, 1172–1178.

O'Regan, B., Grätzel, M., 1991. Nature 353, 737.

Pereira, D.C., Trigueiro, T.G., Colepicolo, P., Marinho-Soriano, E., 2012. Rev. Bras. Farmacogn. 22, 874–880.

Pritchard, D.W., Hurd, C.L., Beardall, J., Hepburn, C.D., 2013. J. Phycol. 49, 867–879.

Radmer, R.J., 1996. BioScience 46, 263–270.

Rasse-Suriani, F.A.O., García-Einschlag, F.S., Rafti, M., Schmidt De León, T., David Gara, P.M., Erra-Balsells, R., Cabrerizo, F.M., 2018. Photochem. Photobiol. 94, 36–51.

Rasse-Suriani, F.A.O., Paula Denofrio, M., Yañuk, J.G., Micaela Gonzalez, M., Wolcan, E., Seifermann, M., Erra-Balsells, R., Cabrerizo, F.M., 2016. Phys. Chem. Chem. Phys. 18, 886–900.

Schmid, M., Guihéneuf, F., Stengel, D.B., 2017. Mar. Biol. 164, 158.

Sepúlveda-Ugarte, J., Brunet, J.E., Matamala, A.R., Martínez-Oyanedel, J., Bunster, M., 2011. J. Photochem. Photobiol. A 219, 211–216.

Shalini, S., Balasundara prabhu, R., Prasanna, S., Mallick, T.K., Senthilarasu, S., 2015. Renew. Sustain. Energy Rev. 51, 1306–1325.

Siller-Sánchez, A., Ruiz, H.A., Aguilar, C.N., Rodríguez-Jasso, R.M., 2019. In: Parameswaran, B., Varjani, S., Raveendran, S. (Eds.), Green Bio-Processes: Enzymes in Industrial Food Processing. Springer Singapore, Singapore, pp. 413–446. http://dx.doi.org/10.1007/978-981-13-3263-0_21.

Stanković, D., Mehmeti, E., Svorc, L., Kalcher, K., 2015. Microchem. J. 118, 95–100.

Teoli, F., Lucioli, S., Nota, P., Frattarelli, A., Matteocci, F., Carlo, A.D., Caboni, E., Forni, C., 2016. J. Photochem. Photobiol. A 316, 24–30.

Tributsch, H., 2004. Coord. Chem. Rev. 248, 1511–1530.

Vásquez-Suárez, A., Lobos-González, F., Cronshaw, A., Sepúlveda-Ugarte, J., Figueroa, M., Dagnino-Leone, J., Bunster, M., Martínez-Oyanedel, J., 2018. PLoS One 13, e0195656.

Švorc, L.u., Cinková, K., Samphao, A., Stanković, D.M., Mehmeti, E., Kalcher, K., 2015. J. Electroanal. Soc. 744, 37–44.

Waaland, J.R., Waal, S.D., Bates, G., 1974. J. Phycol. 10, 193–199.

Wongcharee, K., Meeyoo, V., Chavadej, S., 2007. Sol. Energy Mater. Sol. Cells 91, 566–571.

Yamazaki, E., Murayama, M., Nishikawa, N., Hashimoto, N., Shoyama, M., Kurita, O., 2007. Sol. Energy 81, 512–516.

Yella, A., Lee, H.-W., Tsao, H.N., Yi, C., Chandiran, A.K., Nazeeruddin, M.K., Diau, E.W.-G., Yeh, C.-Y., Zakeeruddin, S.M., Grätzel, M., 2011. Science 334, 629–634.

Yu, Q., Wang, Y., Yi, Z., Zu, N., Zhang, J., Zhang, M., Wang, P., 2010. ACS Nano 4, 6032–6038.

Yum, J.-H., Moon, S.-J., Karthikeyan, C.S., Wietasch, H., Thelakkat, M., Zakeeruddin, S.M., Nazeeruddin, M.K., Grätzel, M., 2012. Nano Energy 1, 6–12.

Zhang, D., Lanier, S.M., Downing, J.A., Avent, J.L., Lum, J., McHale, J.L., 2008. J. Photochem. Photobiol. A 195, 72–80.

Zhou, H., Wu, L., Gao, Y., Ma, T., 2011. J. Photochem. Photobiol. A 219, 188–194.